Published in final edited form as:
J Biomech. 2011 August 11; 44(12): 2279–2285. doi:10.1016/j.jbiomech.2011.05.034.

AGE-RELATED CHANGES IN HUMAN TRABECULAR BONE: RELATIONSHIP BETWEEN MICROSTRUCTURAL STRESS AND STRAIN AND DAMAGE MORPHOLOGY

Jessica M. O'Neal[a,b], **Srinidhi Nagaraja**[a,c], **Tamim Diab**[a], **Brani Vidakovic**[d], and **Robert E. Guldberg**[a,d]

[a]Woodruff School of Mechanical Engineering, Georgia Institute of Technology, Atlanta, GA, 30332 U.S.A.

[b]School of Medicine, Medical College of Georgia, Augusta, GA, 30912 U.S.A.

[c]Center for Devices and Radiological Health, Food and Drug Administration, Silver Spring, MD, 20993 U.S.A.

[d]Wallace H. Coulter Department of Biomedical Engineering, Georgia Institute of Technology, Atlanta, GA, 30332 U.S.A.

Abstract

Accumulation of microdamage in aging and disease can cause skeletal fragility and is one of several factors contributing to osteoporotic fractures. To better understand the role of microdamage in fragility fracture, the mechanisms of bone failure must be elucidated on a tissue-level scale where interactions between bone matrix properties, the local biomechanical environment, and bone architecture are concurrently examined for their contributions to microdamage formation. A technique combining histological damage assessment of individual trabeculae with linear finite element solutions of trabecular von Mises and principal stress and strain was used to compare the damage initiation threshold between pre-menopausal (32–37 years, n=3 donors) and post-menopausal (71–80 years, n=3 donors) femoral cadaveric bone. Strong associations between damage morphology and stress and strain parameters were observed in both groups, and an age-related decrease in undamaged trabecular von Mises stress was detected. In trabeculae from younger donors, the 95% CI for von Mises stress on undamaged regions ranged from 50.7 – 67.9 MPa, whereas in trabeculae from older donors, stresses were significantly lower (38.7 – 50.2, $p<0.01$). Local microarchitectural analysis indicated that thinner, rod-like trabeculae oriented along the loading axis are more susceptible to severe microdamage formation in older individuals, while only rod-like architecture was associated with severe damage in younger individuals. This study therefore provides insight into how damage initiation and morphology relate to local trabecular microstructure and the associated stresses and strains under loading. Furthermore, by comparison of samples from pre- and post-menopausal women, the results

Corresponding Author: Robert E. Guldberg, Ph.D., Institute for Bioengineering and Biosciences, 315 Ferst Drive, Atlanta, GA 30332-0405, robert.guldberg@me.gatech.edu, Phone: (404) 894-6589 Fax: (404) 385-1397.
Jessica O'Neal and Srinidhi Nagaraja have contributed equally to this manuscript.

CONFLICT OF INTEREST
No Disclosures

suggest that trabeculae from younger individuals can sustain higher stresses prior to microdamage initiation.

Keywords

Trabecular bone; Microdamage; Microcomputed tomography; Finite element analysis; Aging; Biomechanics

1. INTRODUCTION

Peak bone mass is reached at approximately age 30, after which a slow decline in bone mass begins throughout the skeleton at rates that vary among individuals and anatomical sites. For trabecular bone in particular, age-related changes include alterations in extracellular matrix heterogeneity and composition (e.g. collagen and noncollagenous proteins, mineral, and water content), quantity (bone volume fraction), remodeling, and microarchitecture (e.g. trabecular thickness, degree of anisotropy, and structural model index). (Hildebrand et al. 1999; Paschalis et al. 2004; Recker et al. 2004; Busse et al. 2009) Of these factors, reductions in bone quantity with corresponding alterations in microarchitecture have been the most extensively studied. Decreased bone volume fraction with age is typically associated with microstructural deterioration in the form of decreased trabecular thickness and connectivity with increased trabecular spacing and anisotropy. (Parfitt et al. 1983; Kimmel et al. 1990).

Alterations in bone mass and microstructure are not the only phenomena that manifest with age. Decreased bone quality is also reflected in an accumulation of unrepaired microdamage. The relationship of microdamage with skeletal fragility has been previously investigated with reports of non-linear increases in crack density with age (Schaffler et al. 1995; Burr et al. 1997; Mori et al. 1997; Fazzalari et al. 1998; Fazzalari et al. 2002). It has been speculated that the accumulation of damage with age may be the result of a breakdown in targeted remodeling of microdamage regions (Burr et al. 2008). However, microdamage does not exclusively occur in aging or disease conditions. Damage and repair of trabeculae are part of the normal turnover and adaptive behavior of bone. It is important to elucidate the mechanisms of crack growth initiation in aging to distinguish normal from pathologic damage formation.

Although age-related degradations in trabecular bone apparent mechanical properties have been well documented, it remains unclear how the local failure properties resulting in microdamage formation in individual trabeculae change with age. A specimen-specific technique was previously developed to assess microstructural stresses and strains associated with microdamage initiation and subsequently applied to different ages of bovine trabecular bone (Nagaraja et al. 2007). In the present study, a more clinically relevant evaluation of microdamage initiation is provided by correlating damage morphology with local stresses in human trabecular bone. Therefore, the goal of this study was to evaluate how age-related degradations in bone quantity and quality affect the local mechanical environment at microdamage initiation. Specifically, the objective was to evaluate changes in the local stresses, microarchitecture, and mineralization associated with trabecular bone microdamage initiation from the distal femur of younger (32–37 years old) and older (71–80 years old) women. We hypothesized that the stress threshold for microdamage initiation is lower in trabecular bone from older females, indicating a loss in bone microarchitecture and quality with aging.

2. METHODS

Specimen preparation

Fresh-frozen (−80°C) trabecular bone cores (18 mm in length, 5 mm in diameter) were harvested from the distal femur of three pre-menopausal (32–37 years old, n=9) and three post-menopausal (71–80 years old, n=9) female cadavers such that the principal material direction was approximately aligned with the loading axis. Based on available medical records, donors selected for this study did not have any prior history of metabolic bone diseases, osteoporotic fractures, or metastatic cancers. Stainless steel endcaps (5 mm depth) were glued to each end of the bone core specimens using cyanoacrylate glue (Prism 401, Loctite, Newington, CT, USA) to minimize the effects of end artifacts on mechanical testing data and prevent movement within the end-caps. (Keaveny et al. 1994) The specimens were wrapped in saline soaked gauze and stored at −20° C for one week until testing. (Linde et al. 1993)

Micro-CT imaging

All specimens were micro-CT imaged (μCT 40, Scanco Medical, Basserdorf, Switzerland) at a voxel resolution of 21 μm. A threshold to distinguish trabecular bone from background was chosen through histogram analysis of grayscale images and remained consistent throughout all evaluations. Automated distance transformation algorithms were used to calculate morphological parameters including bone volume fraction, trabecular thickness, spacing, number, structural model index (SMI), connectivity and trabecular orientation (Hildebrand et al. 1999). Trabecular orientation was measured as the angle from the principal axis of the trabecula to the loading axis. Trabecular bone mineralization (in mg HA/cm^3) was computed from attenuation values of grayscale micro-CT images based on hydroxyapatite (HA) calibration standards. Specifically, for calibration of the linear attenuation coefficient (1/cm) to hydroxyapatite (HA) mineral density (mgHA/cm^3), a cylindrical HA phantom (Scanco Medical, Basserdorf, Switzerland; 38mm diameter) was utilized. This phantom contained known density rods (0, 200, 400, and 800 mgHA/cm^3) embedded in resin. Scans were performed at the X-ray source energy used in this study (45 kVp). A 0.5mm Al filter was used for all scans. Reconstructions also incorporated a beam hardening correction curve.

Mechanical testing

Using a servo-hydraulic mechanical testing system (Mini Bionix 858, MTS Corp.), specimens were preconditioned for 3 cycles to 0.1% strain followed by a uniaxial compression ramp at a rate of 0.5% strain/s to 0.9% (approximately the yield strain as determined by preliminary testing) and held at constant strain for 3 hours. Apparent strain was calculated using an effective gauge length, defined as the exposed length plus half the length embedded in the endcaps (Keaveny et al. 1997). Specimens were immersed in 0.9% physiologic saline plus protease inhibitors (Protease Inhibitor Cocktail Set V, Calbiochem) throughout mechanical testing to prevent tissue degradation.

Labeling, identifying, and classifying microdamage

Microdamage was detected using a sequential fluorescent labeling technique (O'Brien et al. 2002; Lee et al. 2003). Prior to mechanical testing, specimens were stained with 0.02% alizarin complexone for 8 hours at 4° C and atmospheric pressure to label pre-existing microdamage. Pre-existing microdamage included damage created from specimen extraction, exposed calcium in resorption cavities created during bone remodeling, and microdamage sustained *in vivo* prior to death. To improve stain penetration, marrow was removed from specimens prior to staining (WP-72W, WaterPik, USA) and the top endcap

was attached only after staining with alizarin complexone. After mechanical testing, the top endcap was carefully removed from samples using a diamond saw (Isomet 1000, Buehler Ltd., USA) to improve stain penetration. Specimens were then stained with 0.005% calcein for 8 hours at 4° C and atmospheric pressure to label microdamage incurred from mechanical testing.

After staining, specimens were dehydrated in a series of graded alcohols, cleared, and embedded in methyl methacrylate (MMA). Prior to embedding, specimens were secured in custom alignment fixtures to facilitate registration of histological sections to corresponding micro-CT sections for the same specimen. MMA blocks were sectioned into 150–200 μm thick longitudinal slices on a diamond saw and mounted with Eukitt's mounting medium (EM Sciences, USA) onto glass slides.

Microdamage was assessed using 100X magnification (optical resolution: 1.11 μm) in the central four histology sections from each sample. The microdamage analysis region omitted trabeculae immediately adjacent to specimen edges to exclude trabeculae damaged by the coring process or end-cap removal. Pre-existing microdamage area was quantified with grayscale images taken under red epifluorescence. Test-induced microdamage area was quantified with grayscale images taken under green epifluorescence (Image-Pro Plus, Media Cybernetics, USA). For each section, histograms were generated that contained distinct peaks for background, bone, and microdamage, which were then used to select a threshold separating microdamaged pixels from undamaged pixels. A lower threshold was chosen to distinguish bone from background. Damage area was normalized by the total bone area in each section.

Microdamage was identified based on the criteria that cracks are intermediate in size (larger than canaliculi but smaller than vascular channels), have sharp borders, and a focus plane demonstrating depth of field (Burr et al. 1990; Huja et al. 1999). A classification system published by Moore and Gibson was modified to group test-induced damage into three morphological categories: severe, linear, and diffuse damage (Arthur Moore et al. 2002; O'Neal et al. 2010). Severe damage was classified as either microdamage consisting of one primary crack with minor secondary cracks or through-thickness cracks, linear damage included both single and parallel cracks, and diffuse damage consisted of cross-hatch damage that was either equal in length and intensity (to distinguish it from severe damage) or damage with a large area of distribution (Figure 1). Trabeculae exhibiting calcein-stained damage only were selected for finite element analysis (n=100 total trabeculae per age group). In the young group, 44 severe, 20 linear, 17 diffuse, and 19 undamaged trabeculae were analyzed. In the old group, 39 severe, 13 diffuse, 22 linear, and 26 undamaged trabeculae were analyzed.

Finite element analysis

Micro-CT images were used to create 3-D high-resolution finite element (FE) models for estimating the local stress and strain distributions (FEA software, Scanco Medical, Basserdorf, Switzerland). After thresholding the micro-CT images, individual voxels within the images were directly converted into 4–6 million hexahedral finite elements by assigning nodal connectivity and bone tissue properties. Approximately six voxels (21 μm/voxel) spanned the mean trabecular thickness, which provided accurate solution convergence (Guldberg et al. 1998). A conjugate gradient solver with an element-by-element matrix vector multiplication scheme allowed for the estimation of tissue-level stresses and strains (Van Rietbergen et al. 1996). A homogeneous linear isotropic analysis was utilized, and a Poisson's ratio of 0.3 was assumed.

The tissue modulus was back-calculated to match the apparent modulus obtained during testing of the specimens (Van Rietbergen et al. 1995). The back-calculated tissue moduli for the pre-menopausal group were 9.6 GPa (32 year old), 9.2 GPa (37 year old) and 10.7 GPa (37 year old). The back-calculated tissue moduli for the post-menopausal group were 10.5 GPa (71 year old), 10.3 GPa (76 year old) and 9.5 GPa (80 year old). A 0.9% uniaxial compressive strain was placed on the top face of models to simulate loading conditions from the mechanical tests. Von Mises equivalent stresses/strains and maximum compressive principal stresses/strains were extracted from the FE analysis. Microdamaged and undamaged trabeculae identified under green epifluorescence were then visually registered to the same trabeculae within the finite element models (Figure 2 for damaged and Figure 3 for undamaged), and average stress within each extracted trabecula was calculated.

Statistics

One-way ANOVA was used to determine global architectural differences between donors in each age group. Differences due to donor were not significant for most architectural parameters (BV/TV, anisotropy, SMI, trabecular number, and mineralization). Among old donors, trabecular spacing was significantly different ($p=0.04$). Among young donors, trabecular thickness ($p=0.04$) and connectivity ($p=0.05$) were significantly different.

T tests were performed to determine statistically significant differences between age groups for the global architectural parameters reported in Table 1 after verifying normality. For the age and damage category differences in the microstructural mechanical and architectural factors compared in Figures 4, 5, and 6, Kruskal-Wallis nonparametric tests with Mann-Whitney post-hoc pairwise comparisons were run for each combination of damage category and age group to determine significant differences in the interaction. Since this approach may increase the probability of committing a Type I error, a Bonferroni correction was applied to the alpha level for pairwise comparisons within mechanical factors (VM and principal stress and strain) and architectural factors (mineralization, SMI, thickness, and orientation). This reduces the significance level of the tests to 0.0125. All values are reported as mean ± standard error.

3. RESULTS

Global trabecular microarchitecture between age groups, determined by micro-CT evaluation, was similar for most architectural parameters (Table 1). There was a trend for increased trabecular number ($p=0.07$) and decreased trabecular spacing ($p=0.10$) in younger women. Pre-menopausal trabecular bone contained more redundant struts compared to post-menopausal bone ($p=0.01$), and average mineralization for the younger specimens was significantly lower ($p<0.001$) compared to older specimens.

Pre-existing damage area was significantly higher ($p=0.02$) in older specimens (0.0023 ± 0.0004 mm^2/mm^2) compared to pre-menopausal trabecular bone specimens (0.0014 ± 0.0002 mm^2/mm^2). The number of pre-existing severe and diffuse damage incidents was significantly greater in the older group (0.14 ± 0.03 and 0.64 ± 0.09 incidents/mm^2, respectively) than the younger group (0.03 ± 0.01 and 0.23 ± 0.04 incidents/mm^2, respectively; $p<0.003$). The number of pre-existing linear damage incidents was not different (0.71 ± 0.09 incidents/mm^2 in the older group vs. 0.64 ± 0.05 incidents/mm^2 in the younger group). Although test-induced microdamage area in older specimens (0.0131 ± 0.002 mm^2/mm^2) was higher than in younger specimens (0.0108 ± 0.0008 mm^2/mm^2), this difference was only a trend ($p=0.10$). Likewise, levels of severe, linear, and diffuse test-induced damage in the older group (0.48 ± 0.08, 1.67 ± 0.1, 0.82 ± 0.09 incidents/mm^2, respectively) was not significantly different from the younger group (0.59 ± 0.09, 2.03 ± 0.17, 1.03 ± 0.1 incidents/mm^2, respectively). Among test-induced damage, $70.6 \pm 5.8\%$ of

trabecular microdamage in the young group was *de novo* (i.e. no pre-existing microdamage), which was significantly higher than 49.8 ± 2.8% in the old age group ($p=0.03$).

Differences within each age group were found among damaged trabeculae. Severely damaged trabeculae possessed significantly higher von Mises and principal stresses than linear and undamaged trabeculae (Figure 4a and b, $p<0.001$) in both young and old age groups. In older subjects, undamaged trabeculae were under significantly lower von Mises and principal stress than all other damage types ($p<0.001$). A significant decrease in the von Mises stress of undamaged trabeculae in elderly donors compared to undamaged trabeculae in younger donors was observed. ($p<0.01$) and approached significance in the principal stress data ($p=0.014$).

Analysis of von Mises and principal strains revealed similar relationships to the stress results. In the young and old age groups, severely damaged trabeculae possessed von Mises and principal strains that were significantly greater than linear and undamaged trabeculae (Figure 5a and b, $p<0.003$). Diffusely damaged trabeculae in the young age group had greater von Mises and principal strains than linearly damaged and undamaged trabeculae ($p<0.01$). In the older age group, undamaged trabeculae were less strained (von Mises or principal) compared with all other damage types ($p<0.003$). Among undamaged trabeculae, the older age group was less strained than the young group for both strain measures ($p=0.014$ for principal strain, $p=0.013$ for von Mises strain).

Individual trabeculae which underwent micromechanical analysis were also characterized by their structural model index (SMI), trabecular orientation, trabecular thickness, and mineralization to determine whether damaged trabeculae possessed different microarchitecture than undamaged trabeculae (Figure 6). Analysis of the SMI showed that severely damaged trabeculae are more rod-like than undamaged trabeculae in both pre- and post-menopausal groups ($p<0.003$, Figure 6a). Trabecular orientation was assessed to determine whether damage preferentially occurred in trabeculae oriented at particular angles from the loading axis (Figure 6b). In older samples severely damaged trabeculae were more commonly oriented along the longitudinal axis of the specimen in line with the loading axis ($p<0.01$). In younger samples linearly damaged trabeculae were at a significantly greater angle compared to the loading axis than both severe ($p<0.001$) and diffusely damaged ($p=0.001$) samples. When trabecular thickness was examined, severely damaged trabeculae in the older age group were significantly thinner than undamaged trabeculae ($p<0.01$). In the pre-menopausal group, severely damaged trabeculae were thinner than linearly damaged trabeculae ($p<0.01$, Figure 6c). Local mineral density was evaluated (Figure 6d), and severe, diffuse, and undamaged trabeculae were significantly more mineralized in the older age group compared to the younger age group ($p<0.001$).

4. DISCUSSION

In this study, the stress and strain state of damaged and undamaged trabeculae from two groups, females 32–37 years and females 76–80 years, were compared to investigate whether age-related differences existed in the mechanical environment associated with microdamage initiation. Trabecular bone cores were stained with two fluorophores to separate *in vivo* and artifactual damage created from the extraction process from damage incurred during a uniaxial compression loading protocol to the yield strain (0.9%). Trabeculae exhibiting test-induced damage only were registered with solutions of principal and von Mises stresses and strains obtained from linear image-based finite element analysis. Results suggest that microdamage morphology is highly dependent on both the stress and strain magnitude, and that trabecular bone from pre-menopausal women may be able to

sustain higher stresses/strains without damaging compared with trabecular bone from post-menopausal individuals.

It is unclear whether a stress or strain-based criterion for damage initiation is most appropriate, and whether shear forces are significant. In our study, stress values were scaled using a back-calculated tissue modulus unique to each trabecular bone sample. We obtained a similar average tissue modulus between age groups (9.8 GPa for the older group vs 10.2 GPa for the younger group), so our corrections had a small impact on the age-related stress differences. However, in the only age-related difference found among undamaged trabeculae, we observed the greatest differences using von Mises stress to characterize the micromechanical environment. Others have used von Mises stress to define microdamage formation and character, and the association between shear forces and cross-hatched damage morphology has been documented. (Fyhrie et al. 2000; Yeni et al. 2003; Yeni et al. 2008) Thus stress-based criteria with shear factors may be more sensitive to differences between groups than strain-based criteria, depending on the magnitude of the difference between tissue-level stiffness.

Rather than assuming homogeneity in the model, inhomogeneous tissue properties can be assigned based on material attenuation which may improve tissue-level stress and strain predictions. (van Ruijven et al. 2007) Additional FE analyses were performed with inhomogeneous tissue moduli by assigning each voxel in the trabecular structure a tissue modulus based on micro-CT density (data not shown). Each sample was scaled independently and tissue moduli ranged from 7.0–13.2 GPa (32 year old), 7.7–14.0 GPa (37 year old), and 7.1–13.2 GPa (37 year old) for younger donors. Tissue moduli ranged from 7.7–14.4 GPa (71 year old), 7.4–14.2 GPa (76 year old), and 6.8–14.8 GPa (80 year old) for older women. Accounting for variations in elastic modulus resulted in small changes in local stresses (less than 10%) and strains (less than 4%) compared to homogenous analyses for undamaged and damaged trabeculae. This was observed in both younger and older groups and did not alter the conclusions of the study. These data were also in agreement to our previous findings in bovine trabecular bone. (Nagaraja et al. 2007)

We found that the older group had significantly increased levels of pre-existing damage compared with the younger group. Test-induced damage area was not significantly different between age groups, however, and incidents of test-induced damage were actually higher in the younger group compared to the older group. These results indicate that pre-existing damage has an effect on subsequent damage formation. We found it more likely that damage created in uniaxial compression co-localized with pre-existing damage in the older group. These findings have implications for our conclusions. Although the stress and strain values reported were obtained only for *de novo* damage, stress values were scaled according to the back-calculated tissue modulus. The fact that older bone had more pre-existing damage than younger bone results in an unequal deviation from the undamaged stiffness values between the age groups, meaning that the mechanical properties of our undamaged trabeculae in the old group may be underestimated, while the mechanical properties of the damaged trabeculae may be overestimated. Applying a correction would shift undamaged stress values upwards, and decrease damaged stress values, lessening the differences between the groups. Strain values, however, would be unaffected as they are not dependent on the back-calculated tissue modulus.

Analyses into local trabecular architecture revealed that damage severity correlated with trabeculae that were thinner, more rod-like, and oriented closer to the loading axis than their undamaged counterparts. Incorporating these results with local stress/strain data, we observed that damaged trabeculae have higher stresses in part because they are thinner, more slender, and oriented closer to the loading axis. In addition, consistent with previous studies,

we demonstrated that mineral density increases with age. (Paschalis et al. 1997; Boskey et al. 2005; McNamara et al. 2005)

Several important limitations must be considered when interpreting our data. We analyzed replicates from each donor due to the dependence of mechanical parameters on location within the distal femur. In order to obtain averages of tissue level behavior, we created a balanced design in which equal numbers of cores near the cortex and medullary cavity were analyzed. In statistical analyses, damage incidents were considered independent events because all models were linear and did not contain effects of evolving stresses of neighboring trabeculae on the loading environment. The donor effect is therefore random, and accounting for random factors associated with donors in statistical analysis did not affect outcomes. While this strategy allowed us to simultaneously examine trabeculae possessing a wide range of architectural characteristics, more samples from different donors should be analyzed in order to make stronger conclusions about the general population.

Another limitation of our study is the use of a linear FE model, which may impact the magnitude of stresses and strains reported. Non-linear trabecular yielding at the microstructural level would be expected to affect severely damaged trabecular behavior and stress distribution. As this population represented a small percentage of total trabeculae (less than 1%), errors due to linear assumptions are not great enough to alter conclusions of the study.

In conclusion, this study has demonstrated that microstructural stress and strain magnitude is highly associated with the formation of microdamage of different morphologies in two different groups: young and old females. Few age-related differences were found between stress and strain parameters, although analysis of undamaged trabeculae suggests that younger bone may be more able to accommodate higher loads/deformations than older bone.

Research Highlights

- Trabecular stresses and strains associated with microdamage formation were compared by age.
- Stress/strain values were obtained by combining histological assessment with linear FEA.
- Trabeculae from younger donors sustained higher stresses prior to damaging than older donors.
- Thin, rod-like, and vertically oriented trabeculae susceptible to severe damage in older group.

Acknowledgments

This research study was supported by NIH grant R01 AG027249. The micro-CT system was provided by NSF Major Research Instrumentation Award 9977551. The authors would like to thank Karl Jepsen for assistance with this study. The mention of commercial products, their sources, or their use in connection with material reported herein is not to be construed as either an actual or implied endorsement of such products by the Department of Health and Human Services.

REFERENCES

Arthur Moore TL, Gibson LJ. Microdamage accumulation in bovine trabecular bone in uniaxial compression. J Biomech Eng. 2002; 124(1):63–71. [PubMed: 11873773]

Boskey A, Mendelsohn R. Infrared analysis of bone in health and disease. J Biomed Opt. 2005; 10(3) 031102.

Burr DB, Allen MR. Low bone turnover and microdamage? How and where to assess it? J Bone Miner Res. 2008; 23(7):1150–1151. author reply 1152–3. [PubMed: 18348687]

Burr DB, Forwood MR, et al. Bone microdamage and skeletal fragility in osteoporotic and stress fractures. J Bone Miner Res. 1997; 12(1):6–15. [PubMed: 9240720]

Burr DB, Stafford T. Validity of the bulk staining technique to separate artifactual from in vivo bone microdamage. Clin. Orthop. Relat. Res. 1990; 260 305-208.

Busse B, Hahn M, et al. Increased calcium content and inhomogeneity of mineralization render bone toughness in osteoporosis: mineralization, morphology and biomechanics of human single trabeculae. Bone. 2009; 45(6):1034–1043. [PubMed: 19679206]

Fazzalari NL, Forwood MR, et al. Assessment of cancellous bone quality in severe osteoarthrosis: bone mineral density, mechanics, and microdamage. Bone. 1998; 22(4):381–388. [PubMed: 9556139]

Fazzalari NL, Kuliwaba JS, et al. Cancellous bone microdamage in the proximal femur: influence of age and osteoarthritis on damage morphology and regional distribution. Bone. 2002; 31(6):697–702. [PubMed: 12531564]

Fyhrie DP, Hoshaw SJ, et al. Shear stress distribution in the trabeculae of human vertebral bone. Ann Biomed Eng. 2000; 28(10):1194–1199. [PubMed: 11144980]

Guldberg RE, Hollister SJ, et al. The accuracy of digital image-based finite element models. J Biomech Eng. 1998; 120(2):289–295. [PubMed: 10412392]

Hildebrand T, Laib A, et al. Direct three-dimensional morphometric analysis of human cancellous bone: microstructural data from spine, femur, iliac crest, and calcaneus. J Bone Miner Res. 1999; 14(7):1167–1174. [PubMed: 10404017]

Huja SS, Hasan MS, et al. Development of a fluorescent light technique for evaluating microdamage in bone subjected to fatigue loading. J Biomech. 1999; 32(11):1243–1249. [PubMed: 10541076]

Keaveny TM, Pinilla TP, et al. Systematic and random errors in compression testing of trabecular bone. J Orthop Res. 1997; 15(1):101–110. [PubMed: 9066533]

Keaveny TM, Wachtel EF, et al. Differences between the tensile and compressive strengths of bovine tibial trabecular bone depend on modulus. J Biomech. 1994; 27(9):1137–1146. [PubMed: 7929463]

Kimmel DB, Recker RR, et al. A comparison of iliac bone histomorphometric data in post-menopausal osteoporotic and normal subjects. Bone Miner. 1990; 11(2):217–235. [PubMed: 2268749]

Lee TC, Mohsin S, et al. Detecting microdamage in bone. J Anat. 2003; 203(2):161–172. [PubMed: 12924817]

Linde F, Sorensen HC. The effect of different storage methods on the mechanical properties of trabecular bone. J Biomech. 1993; 26(10):1249–1252. [PubMed: 8253829]

McNamara LM, Prendergast PJ. Perforation of cancellous bone trabeculae by damage-stimulated remodelling at resorption pits: a computational analysis. Eur J Morphol. 2005; 42(1–2):99–109. [PubMed: 16123029]

Mori S, Harruff R, et al. Trabecular bone volume and microdamage accumulation in the femoral heads of women with and without femoral neck fractures. Bone. 1997; 21(6):521–526. [PubMed: 9430242]

Nagaraja S, Lin AS, et al. Age-related changes in trabecular bone microdamage initiation. Bone. 2007; 40(4):973–980. [PubMed: 17175210]

O'Brien FJ, Taylor D, et al. An improved labelling technique for monitoring microcrack growth in compact bone. J Biomech. 2002; 35(4):523–526. [PubMed: 11934422]

O'Neal JM, Diab T, et al. One year of alendronate treatment lowers microstructural stresses associated with trabecular microdamage initiation. Bone. 2010; 47(2):241–247. [PubMed: 20483387]

Parfitt AM, Mathews CH, et al. Relationships between surface, volume, and thickness of iliac trabecular bone in aging and in osteoporosis. Implications for the microanatomic and cellular mechanisms of bone loss. J Clin Invest. 1983; 72(4):1396–1409. [PubMed: 6630513]

Paschalis EP, Betts F, et al. FTIR microspectroscopic analysis of normal human cortical and trabecular bone. Calcif Tissue Int. 1997; 61(6):480–486. [PubMed: 9383275]

Paschalis EP, Shane E, et al. Bone fragility and collagen cross-links. J Bone Miner Res. 2004; 19(12): 2000–2004. [PubMed: 15537443]

Recker R, Lappe J, et al. Bone remodeling increases substantially in the years after menopause and remains increased in older osteoporosis patients. J Bone Miner Res. 2004; 19(10):1628–1633. [PubMed: 15355557]

Schaffler MB, Choi K, et al. Aging and matrix microdamage accumulation in human compact bone. Bone. 1995; 17(6):521–525. [PubMed: 8835305]

Van Rietbergen B, Weinans H, et al. Computational strategies for iterative solutions of large FEM spplications employing voxel data. Int. J. Numer Methods Eng. 1996; 39:2743–2767.

Van Rietbergen B, Weinans H, et al. A new method to determine trabecular bone elastic properties and loading using micromechanical finite-element models. J Biomech. 1995; 28(1):69–81. [PubMed: 7852443]

van Ruijven LJ, Mulder L, et al. Variations in mineralization affect the stress and strain distributions in cortical and trabecular bone. J Biomech. 2007; 40(6):1211–1218. [PubMed: 16934818]

Yeni YN, Hou FJ, et al. Trabecular shear stresses predict in vivo linear microcrack density but not diffuse damage in human vertebral cancellous bone. Ann Biomed Eng. 2003; 31(6):726–732. [PubMed: 12797623]

Yeni YN, Zelman EA, et al. Trabecular shear stress amplification and variability in human vertebral cancellous bone: relationship with age, gender, spine level and trabecular architecture. Bone. 2008; 42(3):591–596. [PubMed: 18180212]

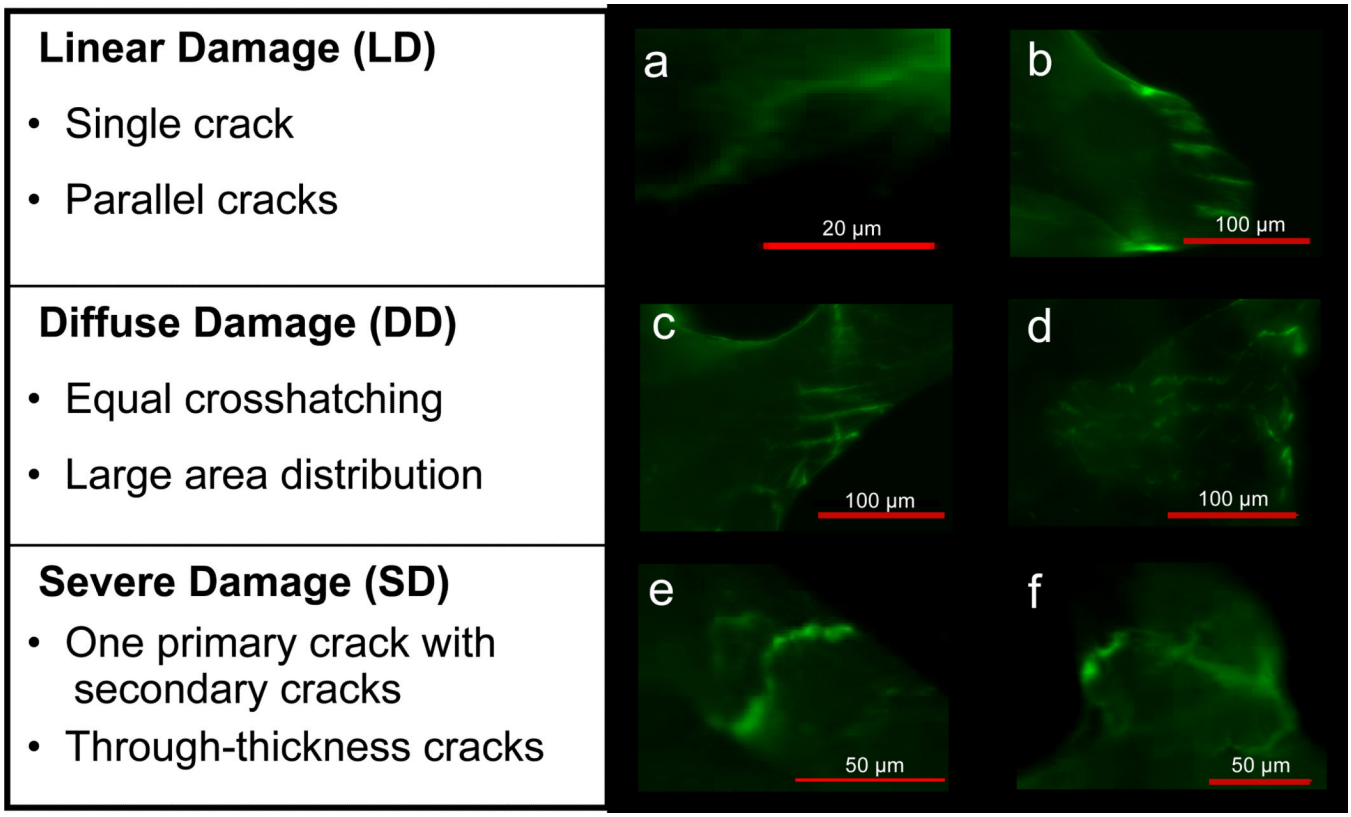

Figure 1.
Damage was separated into three categories based on morphology. Bullet points indicate metrics used to categorize individual trabeculae.

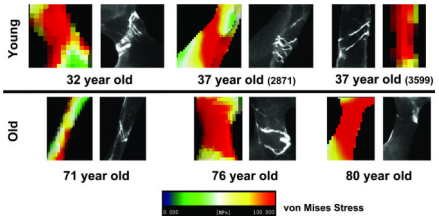

Figure 2.
Representative microdamaged trabeculae extracted from histology sections and homogeneous finite element models (von Mises effective stress shown) for young and old donors.

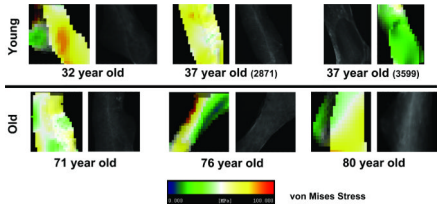

Figure 3.
Representative undamaged trabeculae extracted from histology sections and homogeneous finite element models (von Mises effective stress shown) for young and old donors.

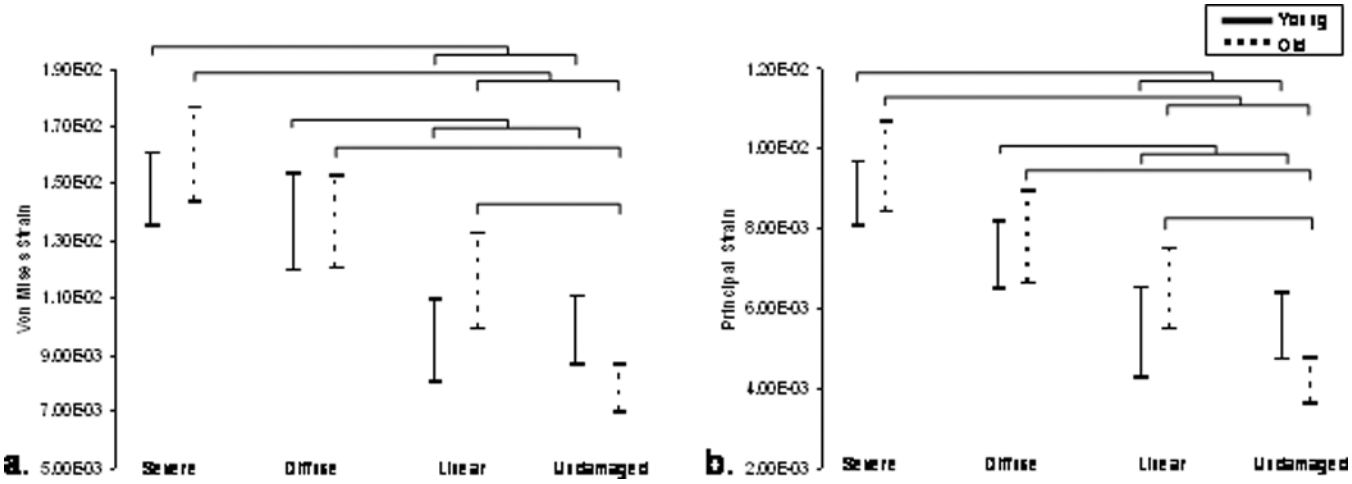

Figure 4.

The 95% confidence intervals for **a.** von Mises and **b.** principal compressive stress initiation ranges calculated by damage category are shown. A significantly greater stress range is demonstrated in young, undamaged trabeculae compared with old, undamaged trabeculae. Significant increases are also seen in the stress state of severely damaged trabeculae compared to linear and undamaged trabeculae in both age groups. Bars represent significant differences ($p<0.01$).

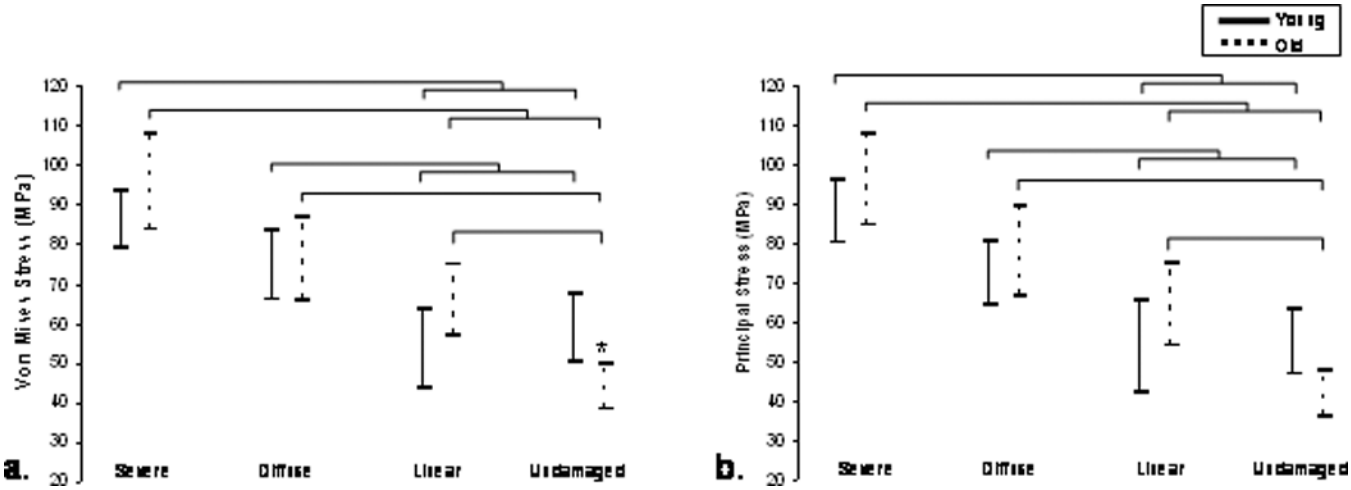

Figure 5.

The 95% confidence intervals for **a.** von Mises and **b.** principal compressive strain initiation ranges calculated by damage category are shown. Significant increases were seen in the strain state of severely damaged trabeculae compared to linear and undamaged trabeculae in both age groups. Bars represent significant differences ($p \leq 0.01$).

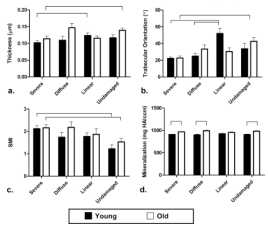

Figure 6.

Trabecular bone microarchitecture and mineralization for young (32–37 year old) and old (71–80 year old) age groups. **a.** Trabecular thickness is plotted, indicating that severely damaged trabeculae are thinner than undamaged in the older age group, and thinner than linearly damaged trabeculae in the younger age group ($p<0.01$). **b.** Trabecular orientation relative to the loading axis is plotted, indicating that in the older age group, trabeculae aligned more acutely with the loading axis is more likely to sustain severe damaged compared to undamaged trabeculae. **c.** SMI is plotted, showing more rod-like trabecular architecture in severely damaged trabeculae compared to undamaged trabeculae in both groups ($p<0.01$). **d.** In severely damaged, diffusely damaged, and undamaged trabeculae, the trabecular mineralization was significantly increased in the post-menopausal group ($p<0.01$).

Table 1

Global Architecture and Mineralization

Parameter	Young	Old	p-value
BV/TV	0.212 (0.012)	0.198 (0.021)	0.42
Tb.Th (μm)	153.9 (12.0)	153.3 (9.0)	0.48
DA	1.87 (0.14)	2.00 (0.13)	0.27
SMI	1.03 (0.11)	0.93 (0.14)	0.3
Tb.N (mm^{-1})	1.57 (0.04)	1.45 (0.07)	0.07
Tb.Sp (mm)	0.58 (0.02)	0.64 (0.03)	0.1
Conn.D	7.21 (0.54)	5.17 (0.62)	0.01
Mineralization (mg HA/cc)	1022.0 (7.5)	1062.8 (6.7)	<0.001